

ELECTROLYTE OPTIMIZATION STUDY FOR TiO<sub>2</sub> NANOTUBE ELECTRODE  
IN SODIUM ION BATTERIES

by

Richard Wendel Cutler

A thesis

submitted in partial fulfillment

of the requirements for the degree of

Master of Science in Materials Science and Engineering

Boise State University

December 2015

© 2015

Richard Wendel Cutler

ALL RIGHTS RESERVED

BOISE STATE UNIVERSITY GRADUATE COLLEGE

**DEFENSE COMMITTEE AND FINAL READING APPROVALS**

of the thesis submitted by

Richard Wendel Cutler

Thesis Title: Electrolyte Optimization Study for TiO<sub>2</sub> Nanotube Electrode in Sodium Ion Batteries

Date of Final Oral Examination: 12 June 2015

The following individuals read and discussed the thesis submitted by student Richard Wendel Cutler, and they evaluated his presentation and response to questions during the final oral examination. They found that the student passed the final oral examination.

Hui (Claire) Xiong, Ph.D.	Chair, Supervisory Committee
Jeunghoon Lee, Ph.D.	Member, Supervisory Committee
Dmitri Tenne, Ph.D.	Member, Supervisory Committee

The final reading approval of the thesis was granted by Hui (Claire) Xiong, Ph.D., Chair of the Supervisory Committee. The thesis was approved for the Graduate College by John R. Pelton, Ph.D., Dean of the Graduate College.

DEDICATION

For Ivan and John Alfred

## ACKNOWLEDGEMENTS

My path to the completion of my formal education has been unexpected and unpredictable but I haven't walked it alone. Many people have assisted me with my research, my course work, and/or provided encouragement along the way. I am grateful for their help. I also would like to thank some individuals specifically.

I thank my parents. Their support has been indispensable in my journey. They have provided financial assistance when I needed it and constant emotional support and encouragement.

I thank my grandparents for making education a priority in my life by making it a priority in my parents' lives.

I thank Chad Watson for helping me get into Boise State University. He befriended me, helped me to adjust to a new university, and then graciously helped me to navigate the forms necessary to change my degree track after my goals changed.

I also owe a debt of gratitude to my advisor Dr. Claire Xiong. Her patient guidance has helped me to grow as an engineer. She set standards for my work that stretched me and helped me to learn to work beyond what I thought were my limitations. She also encouraged me to think about the direction my life is going, rather than just going along for the ride. And, when I did, she supported my changing goals.

Thank You.

## AUTOBIOGRAPHICAL SKETCH OF AUTHOR

Richard Cutler has completed two Bachelor's degrees at the University of Utah (U of U), graduating in 2009. While at the U of U he majored in Materials Science and Engineering, and Metallurgical Engineering. He also worked in a Metallurgy lab on electrowinning and solvent extraction projects. To complete his education at the U of U, he researched and then wrote a thesis on Dimensionally Stabilized Anodes.

After graduating from the U of U, he started a Master's degree program at The Ohio State University. He graduated in 2011 with a Master of Science in Materials Science and Engineering. While at Ohio State, he studied the phase stability of Nickel Superalloys, particularly at the boundaries between dissimilar alloys. He wrote his thesis on phase diagrams for the Ni-Al-Cr and Ni-Al-Mo ternary systems at 1200° C.

Upon graduating from The Ohio State University, Richard interned with Pratt and Whitney Rocketdyne in Los Angeles County, California. While at Rocketdyne, he worked on a team to return the RS-68 engine to production after a plating fault stopped the line. He also assisted the team that was studying the potential replacement chemicals for the nitric acid that was currently used.

After the internship was completed, Richard returned to academia and started studying at Boise State University. He is graduating with a Master of Science in Materials Science and Engineering in 2015.

## ABSTRACT

Batteries are ubiquitous in daily life. Sodium-ion batteries have the potential to become inexpensive alternatives to the current market products such as Lithium-ion batteries.  $\text{TiO}_2$  nanotubes have proven potential as an anode for Na-ion batteries. Electrolytes made by  $\text{NaClO}_4$  salt and carbonate-based solvents make up commonly used electrolytes in sodium ion battery research. We used electrochemical and physical characterization tests to evaluate the optimum electrolyte for this anode material in the Na system. We determined that the  $\text{ClO}_4^-$  ion decomposes at the  $\text{TiO}_2$  surface and promotes the formation of an unstable solid electrolyte interphase. A salt more stable than  $\text{NaClO}_4$  needs to be researched in the electrolyte for future use with  $\text{TiO}_2$  anodes in sodium-ion batteries.

## TABLE OF CONTENTS

DEDICATION .....	iv
ACKNOWLEDGEMENTS .....	v
AUTOBIOGRAPHICAL SKETCH OF AUTHOR .....	vi
ABSTRACT .....	vii
LIST OF TABLES .....	x
LIST OF FIGURES .....	xi
LIST OF ABBREVIATIONS.....	xiii
CHAPTER ONE: INTRODUCTION.....	1
1.1 Background.....	1
1.2 Research Project.....	6
CHAPTER TWO: EXPERIMENTAL PROCEDURE.....	9
2.1 Materials Preparation .....	9
2.2 TiO <sub>2</sub> NT Characterization.....	10
2.3 Electrochemical Characterization Methods .....	10
2.4 Physical Characterization Methods.....	11
CHAPTER THREE: RESULTS AND DISCUSSION.....	13
3.1 TiO <sub>2</sub> NT Characterization.....	13
3.2 Water Content in Electrolytes .....	14
3.3 Electrochemical Characterization .....	15

3.4 Physical Characterization.....	27
CHAPTER FOUR: CONCLUSIONS.....	34
REFERENCES .....	36

## LIST OF TABLES

Table 1	Dielectric constants of the organic solvents used in the electrolyte optimization <sup>67,68</sup> .....	7
Table 2	Half-cell states during each EIS measurement .....	11
Table 3	Results of Karl Fischer Titrations .....	14
Table 4	Bonding information of the FT-IR peaks seen in the measured spectra...	28

## LIST OF FIGURES

<i>Figure 1</i>	Cross-section of an experimental half-cell battery. This type of batter was utilized in the current work.....	2
<i>Figure 2</i>	Sample prepared for RAMAN measurements in hermetically sealed pouch.....	12
<i>Figure 3</i>	Top view of TiO <sub>2</sub> NTs in SEM.....	13
<i>Figure 4</i>	Side view of TiO <sub>2</sub> NTs in SEM .....	14
<i>Figure 5</i>	Half-cells of TiO <sub>2</sub> NTs vs Na/Na <sup>+</sup> . A) Electrochemical capacity of the half cells. B) Coulombic efficiency of the half cells. ....	15
<i>Figure 6</i>	Voltage profiles of the measured electrochemical performance on cycling the half-cells. Displayed are the 1 <sup>st</sup> , 2 <sup>nd</sup> , and 30 <sup>th</sup> cycles. All electrolytes tested are reported here.....	17
<i>Figure 7</i>	Cyclic Voltammetry Data, all electrolytes tested are reported here. ....	19
<i>Figure 8</i>	EIS measurements of the uncycled half-cells. Insert shows the origin in greater detail. Section 1 is the high frequency region. The high frequency region describes the behavior of the bulk electrolyte. Section 2 is the medium frequency region. The medium frequency region shows the interface and interface reactions. Section 3 is the low frequency region, which indicates the diffusion in the solid electrode.....	20
<i>Figure 9</i>	EIS measurements for half-cell with PC electrolyte. The insert shows the origin with greater detail. ....	22
<i>Figure 10</i>	EIS measurements for half-cell with EC:PC electrolyte. The insert shows the origin with greater detail. ....	23
<i>Figure 11</i>	EIS measurements for half-cell with EC:EMC electrolyte. The insert shows the origin with greater detail. ....	24
<i>Figure 12</i>	EIS measurements for half-cell with EC:DMC electrolyte. The insert shows the origin with greater detail. ....	25

<i>Figure 13</i>	EIS measurements for half-cell with EC:DEC electrolyte. The insert shows the origin with greater detail. ....	26
<i>Figure 14</i>	FT-IR spectra for the electrodes after one complete discharge/charge cycle for each of the electrolytes tested. ....	28
<i>Figure 15</i>	FT-IR data at low wavenumbers. The dotted line marks the C-Cl bond.....	29
<i>Figure 16</i>	Raman spectra for TiO <sub>2</sub> electrodes in charged state. Two electrolytes were tested, EC:EMC and EC:DMC. ....	31
<i>Figure 17</i>	XPS data from half-cell with PC electrolyte, focused on the Cl spectra collected. The black line and circles shows the data collected by the XPS. The fitted peaks 1-4 are the identified peaks in the spectra and the cumulative peak fit in green shows that the fit matches the data .....	32

## LIST OF ABBREVIATIONS

PC	Propylene Carbonate
EC	Ethylene Carbonate
DMC	Dimethyl Carbonate
DEC	Diethyl Carbonate
EMC	Ethyl Methyl Carbonate
FEC	Fluoroethylene Carbonate
SEI	Solid-Electrolyte Interface
Li	Lithium
Li-ion	Lithium ion
Na	Sodium
Na-ion	Sodium ion
NaClO <sub>4</sub>	Sodium Perchlorate
NaPF <sub>6</sub>	Sodium Hexafluorophosphate
Ti	Titanium
TiO <sub>2</sub>	Titanium Dioxide
FePO <sub>4</sub>	Iron Phosphate
CrPO <sub>4</sub>	Chromium Phosphate
DI water	Deionized water
IPA	Isopropyl Alcohol
M	Molar
ppm	Parts per Million

## CHAPTER ONE: INTRODUCTION

### 1.1 Background

Batteries are ubiquitous in daily life. Lithium-ion (Li-ion) batteries have been used in consumer electronics since they were introduced to the market by SONY Corporation in the 1990s<sup>1</sup>. Li-ion batteries are preferred in consumer electronics because they have the highest energy density among commercially available primary and rechargeable battery technologies. In addition, due to their high energy densities, Li-ion batteries have been introduced into the automobile market to power the next generation electric vehicles. Li-ion batteries are also being used as stationary power supplies for large-scale grid applications. The increasing demands of these markets raises the question of whether these demands could be met by the global lithium reserves. Moreover, the majority of the global lithium reserves are located in South America<sup>2</sup>. This inequitable distribution has the potential to lead to a new collective of resource-rich countries on whom resource-poor countries must depend. An alternative energy storage system is needed; Sodium-ion (Na-ion) batteries can potentially answer these concerns.

Na-ion batteries are a promising alternative to Li-ion batteries. Both Li and Na are alkaline metals. Na has many properties in common with Li because of its proximity on the periodic table. Sodium is also available at significantly lower cost<sup>2</sup>. Finally, Na is readily available in the oceans, inland seas, and dry lake beds, which gives easy access to anyone who wants it<sup>3</sup> and could alleviate some of the geopolitical tensions that currently

exist because of energy politics. For these reasons, Na-ion batteries are being investigated as an attractive alternative.

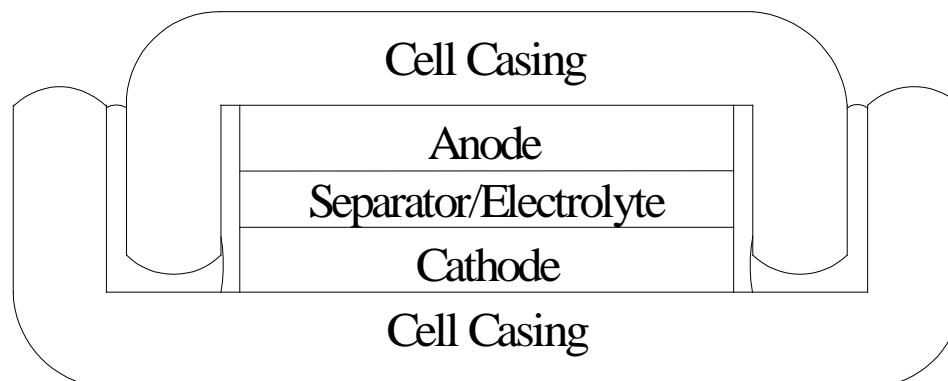


**Figure 1** Cross-section of an experimental half-cell battery. This type of battery was utilized in the current work.

General battery configuration includes four major components: Anode, Cathode, Electrolyte, and Separator (as seen in *Figure 1*). The anode and cathode are the electrodes where the oxidation and reduction half-reactions occur during operation. The separator is between the anode and the cathode. The separator must be capable of physically preventing the anode and cathode from making contact to cause short circuit. The separator must also be porous to allow the electrolyte to pass through and contact both electrodes simultaneously. The electrolyte provides ionic transportation between the two electrodes while at the same time providing an electrical barrier between them. In the interior of a battery, charge is carried by ions moving through the electrolyte. Ionic mobility in the electrolyte is an important property because if the mobility is low then the battery will only be capable of slow discharges and charges and consequently the power of the battery is low. The electrode/electrolyte interfaces are also extremely important. The rate of charge transfer across the interface impacts charge and discharge rates. The presence of side reactions between the electrode and electrolyte at the interface can

significantly affect battery operations and cycle life. The solid electrolyte interface (SEI) formed at the electrode surface might block the passage of ions to reduce the capacity of a battery. Nevertheless, a stable SEI with capability to let ions pass through can act as a protection layer of reactive electrode from further attack by electrolyte. As research is done to develop new batteries, some requirements are universal; all battery components need to be as non-toxic and environmentally benign as possible. Ideally the materials used would also be recyclable and be produced using low energy processing techniques.

As electrode properties significantly affect the performance of a battery, enormous research efforts have been invested in electrode materials discovery, design, and optimization. A few suitable anode and cathode materials have been identified for the Na-ion system. Because of the similarities in the chemistry for Li and Na, the electroactive materials can often work in both system. Carbon<sup>4-11</sup>, Tin<sup>12,13</sup>, and TiO<sub>2</sub><sup>14</sup> have been identified as promising anode systems and oxides of Cobalt<sup>15</sup>, Manganese<sup>16,17</sup>, Vanadium<sup>18,19</sup>, and FePO<sub>4</sub><sup>20,21</sup>, CrPO<sub>4</sub><sup>22</sup>, and some mixed oxides<sup>23-27</sup> have all been identified as cathode materials for Na-ion batteries.

Carbon electrode research has reported up to 300 mAh/g capacity<sup>5</sup> for anodes while exploring different precursors: pitch based carbon<sup>4</sup>, glucose<sup>5</sup>, carbon black<sup>28</sup>, graphene<sup>29</sup>, and expanded graphite<sup>30</sup> to name a few, and processing methods<sup>6,8,10</sup>. Graphene<sup>29</sup> and expanded graphite<sup>30</sup> have both demonstrated capacity for extended cycles. Research in Sn, Sb, and Sn alloys focuses on identifying the desirable phases<sup>31,13,32,33</sup>. The other major emphasis in Sn research is in reducing diffusion distances inside the electrode by reducing the electrode particle size<sup>12,34,32,35</sup>. In the cathode research, research groups are exploring manganese oxide to determine the

structure, increase capacity, and facilitate Na ion mobility in the material<sup>13,23,36-38</sup>.

Vanadium oxide research is concentrated on the stoichiometry and structure as well as processing nano-scale features<sup>22,19,39,18,40,41</sup>. Research into FePO<sub>4</sub>, similar to manganese oxides, is focused on material structure and processing to reduce particle size and diffusion distance<sup>20,21,42-44</sup>.

TiO<sub>2</sub> research is ongoing into the various crystal structure polymorphs: anatase<sup>45</sup>, amorphous<sup>14</sup>, bronze<sup>46</sup>, hexagonal<sup>47</sup>, and monoclinic<sup>48</sup> and have reported capacities as high as 240 mAh/g<sup>49</sup> for Na-ion batteries. TiO<sub>2</sub> has been used in a wide variety of products and is readily available in the marketplace, and the mature supply chain should keep material costs low. TiO<sub>2</sub> also has multiple processing options. TiO<sub>2</sub> based anode materials can be easily produced by several different methods: electrochemical<sup>14,45</sup>, pyrolysis<sup>47,48,50</sup>, and hydrolysis<sup>46,51</sup>. Electrochemical processing is desirable because it is simple and scalable, which facilitates both researching the material and industrial scale production. Electrochemical processing is flexible in the production of nano-scale features, and facile nano tube growth has been demonstrated<sup>14</sup>. Similar to the concerns in Sn, Manganese oxides, Vanadium oxides, and FePO<sub>4</sub>, Na-ion mobility and diffusion distances in the TiO<sub>2</sub> structure affect the performance of the electrode. Reducing the diffusion distance increases the rate of diffusion, and diffusion rate has a dramatic effect on electrode performance<sup>52</sup>. Ion movement into NTs moves perpendicular to the long axis of the NTs, reducing the diffusion distance to a maximum of the NT wall thickness. TiO<sub>2</sub> NT anodes in Na-ion batteries have the potential to become an inexpensive, high performance replacement for current technology based on Li-ions.

Since interfaces between the electrodes and the electrolyte play a critical role in battery stability, it is important to research the surface science of batteries. Reactions are sensitive to and specific to the surface present, and may or may not proceed on the exposed surface<sup>9</sup>. The reactions that occur at the interface should include the charge conducting ion crossing the interface, but may also include the formation of a SEI. A SEI is a layer of surface deposits that form from decomposition products produced by electrolyte reactions at the surface of the electrode. The electrode acts as a catalyst or reactant for these reactions. The SEI can be stable or unstable and reform during each cycle. It can improve capacity, have no discernable effect, or it can degrade the capacity and shorten the life of the battery. Altering the surface chemistry of an electrode can lead to faster charge transfer across the interface and/or ion diffusion into the electrode<sup>52-55</sup>. Because of the reactivity of the electrode surface, electrolytes are usually individually matched to the electrodes. An ideal electrolyte will have very high ionic conductivity, fully wet the electrode surfaces, have a wide electrochemical window, have no extraneous reactions internally or with the electrode, and will be inert to other cell components (separator, etc.). In order to meet such requirements, the electrolyte must be optimized for each electrode system individually. Ponrouch *et al.* have worked on the hard carbon system and identified 1 Molar (M) sodium hexafluorophosphate ( $\text{NaPF}_6$ ) in ethylene carbonate:propylene carbonate (EC:PC) as an excellent electrolyte, exhibiting greater stability on cycling up to 120 cycles<sup>56,57</sup>. Their further investigations have shown that by adding 10% dimethyl carbonate (DMC), the SEI was stabilized with good Coulombic efficiency, 98.5%, over 100 cycles<sup>11</sup>. Bhide *et al.* worked on the cobalt oxide ( $\text{CoO}_2$ ) system and discovered that using  $\text{NaPF}_6$  produced an electrochemically stable

SEI during battery cycling<sup>58</sup>. Vidal-Abarca *et al.* studied the iron phosphate ( $\text{FePO}_4$ ) system; they identified EC:diethyl carbonate (DEC) with  $\text{NaPF}_6$  as the best electrolyte in this system because it lead to the highest Coulombic efficiency and the greatest capacity retention while cycling<sup>59</sup>. Komaba *et al.* worked with nickel/ manganese oxide ( $(\text{Ni,Mn})\text{O}_2$ ) and determined that fluoroethylene carbonate (FEC) is an effective additive for PC electrolytes because the FEC improves electrolyte stability, leading to greater capacity retention<sup>60</sup>. Our previous work on a computational analysis with experimental corroboration of electrolyte solvent analysis in the  $\text{TiO}_2$  system has found that EC:PC would make the most optimized electrolytes<sup>61</sup>. Wu *et al.* also studied electrolytes in the  $\text{TiO}_2$  system, focusing on electrolyte salts, and found that the performance of a  $\text{TiO}_2$  electrode is dependent on the electrolyte present<sup>62</sup>. Wu *et al.* further recommend using  $\text{NaClO}_4$  as the salt in electrolytes for  $\text{TiO}_2$  anodes.

## 1.2 Research Project

In this work, we investigated the performance of  $\text{TiO}_2$  nanotubes (NTs) with several different electrolytes.  $\text{TiO}_2$  is a material commonly found in applications as diverse as paints, solar cells, and pharmaceuticals, because  $\text{TiO}_2$  is chemically inert and non-toxic and environmentally benign<sup>63</sup>. We have previously shown that  $\text{TiO}_2$  NTs have potential in Na-ion battery applications due to phase stability and promising specific capacity,  $150 \text{ mAh/g}^{14}$ . NTs are easy to produce by electrochemical anodization<sup>64-66</sup>. Anodization allows fine control on both the diameter and the length of the NTs<sup>66</sup>. Surface finish can also be controlled<sup>65</sup>. Furthermore, the NTs have greatly increased surface area, which can improve the reaction kinetics<sup>65</sup>.

The electrolytes that we tested were all carbonate-based liquid solutions with 1M sodium perchlorate ( $\text{NaClO}_4$ ) salt. Carbonate liquids are commonly used for Li and Na electrolytes and are readily available in high purity. In our previous work, we have determined theoretically that  $\text{NaClO}_4$  in binary carbonate solvents would have several attractive properties for an electrolyte: low viscosity, high ionic conductivity and low ionic solvation energies<sup>61</sup>. We have also identified EC:PC, EC:EMC, and EC:DMC as the electrolytes that will have the best theoretical performance. We are building on this foundation by experimentally determining the performance of these three electrolytes as well as PC and EC:DEC from theoretical calculations and simulations.

**Table 1 Dielectric constants of the organic solvents used in the electrolyte optimization<sup>67,68</sup>.**

Organic Solvent	Dielectric Constant	Viscosity (cP, 25° C)
Propylene Carbonate (PC)	64.9	2.53
Ethylene Carbonate (EC)	89.8	1.90 (40° C)
Dimethyl Carbonate (DMC)	3.1	0.59 (20° C)
Diethyl Carbonate (DEC)	2.8	0.75
Ethyl Methyl Carbonate (EMC)	3.0	0.65

Table 1 shows the dielectric constants and viscosities of the individual solvents used. The dielectric constant will be directly related to the solubility limit of the salt in the solution. The ability of the electrolyte to wet the surface of the electrode will be, in part, inversely related to the viscosity of the electrolyte. PC and EC have the highest dielectric constants, making them desirable for investigation. DMC, DEC, and EMC

have significantly lower dielectric constants, however, they have low viscosities. DMC, DEC, and EMC are all thinner than water. In order to capitalize on the high dielectric constant of EC but reduce the problems associated with the higher viscosity, mixtures of EC:DMC, EC:DEC, and EC:EMC are being investigated.

Our focus is on characterizing the electrode and electrolyte behaviors by utilizing electrochemical and physical methods. We will use the electrochemical methods to quantify the material capacity and the electrolyte stability. We will use the physical methods to determine the compositions of any SEIs that form on the surface of the electrodes. We will compare the data generated from all of the tests to determine the stability of the electrolytes and the SEIs that are formed. By quantifying the electrode material capacity, the electrolyte stability, and the formation/stability of any SEI, we expect to be able to determine the optimal electrolyte and make recommendations for further work.

## CHAPTER TWO: EXPERIMENTAL PROCEDURE

### 2.1 Materials Preparation

All chemicals were purchased from Sigma Aldrich and +99% pure unless otherwise noted. All procedures and tests were run at ambient temperature. The electrolytes were mixed and handled in an Argon-filled glovebox from MBraun. The solvents used in the electrolytes were propylene carbonate (PC) and combinations of PC with ethylene carbonate (EC), dimethyl carbonate (DMC), diethyl carbonate (DEC), and ethyl methyl carbonate (EMC). The solvent combinations were all in a 1:1 ratio by volume. The solvents volumes were measured using an analytical scale to achieve greater accuracy. After the solvents were mixed, NaClO<sub>4</sub> salt was added to the solvents and allowed to dissolve in a covered container to prepare for a 1M solution. Electrolytes were stirred using a magnetic stir bar for several hours to ensure complete dissolution of the salt prior to being used in half-cells. The electrolytes were titrated with a Mettler Toledo C30 Karl Fischer coulometer (in the glovebox) to determine the water content of each of the electrolytes.

The TiO<sub>2</sub> NTs used as electrodes were synthesized by electrochemical anodization with a previously reported method<sup>14,64,69,61</sup>. The titanium (Ti) foil was cleaned by rinsing in acetone, isopropyl alcohol (IPA), and deionized (DI) water for 5 minutes in sequence in a sonicator. After the surface had been cleaned and dried, the back of the foil was covered with tape to confine the anodization to one side of the foil and to ensure uniform current distribution during anodization. Foils were anodized in a

formamide solution with 5% DI water (by volume) and 0.8wt% ammonium fluoride. The Ti foil was anodized in a two electrode cell, as the working electrode, with a platinum mesh counter electrode and a potential of 25 V for 30 minutes. After anodization, the Ti foil was rinsed in DI water and sonicated for 15 seconds. The foil was then immersed in IPA and subsequently annealed in a vacuum furnace at 110° C overnight.

Na half-cells were assembled using coin-type cells (Hohsen 2032) with TiO<sub>2</sub> NTs as the working electrode and pure sodium metal as the counter electrode, with a glass fiber separator (Whatman GF/F). TiO<sub>2</sub> NT electrodes were punched out with a 9/16” punch, weighed and then dried in a vacuum furnace at 110° C for an hour prior to moving them into the glovebox for assembly. No carbon additives or polymer binders were used because the nanotubes were grown directly on Ti foil and remained attached, which allowed the Ti foil to act as a current collector. The half-cells were assembled and sealed in an Ar-filled glovebox (H<sub>2</sub>O, O<sub>2</sub><0.5 ppm).

## **2.2 TiO<sub>2</sub> NT Characterization**

TiO<sub>2</sub> NT length and opening diameter were determined using a JEOL JSM-7500F field emission SEM operating at 10kV.

## **2.3 Electrochemical Characterization Methods**

The battery cycling performance of the as prepared electrode was investigated by a Maccor battery tester. The half cells were galvanostatically cycled between 2.5 and 0.5 V vs Na/Na<sup>+</sup>. The cycling was done at a current of 16mA/g for all of the samples. Each sample was subjected to 30 cycles.

Cyclic Voltammetry (CV) and Electrochemical Impedance Spectroscopy (EIS) measurements were made using a CH Instruments Electrochemical Workstation

(CHI660D). Fresh half-cells were tested in each of these tests. The half-cells were cycled between 2.5 and 0.5 V vs Na/Na<sup>+</sup> with a scan rate of 0.1 mV/sec for the CV measurements. Each sample was recorded for 5 cycles. The EIS tests were conducted from 10<sup>5</sup> to 10<sup>-3</sup> Hz with an amplitude of 5 mV. EIS measurements were made on virgin half-cells. After the initial measurements, the half-cells were discharged to 0.5 V on the Maccor battery tester at 16mA/g and then a second set of EIS tests were conducted. The half-cells were then charged to 2.5 V on the Maccor battery tester at 16mA/g and EIS measurements were then taken for a third time. This cycle was repeated to acquire EIS measurements for the fourth and fifth time. The state of charge for the half-cell during each EIS measurement can be seen in Table 2.

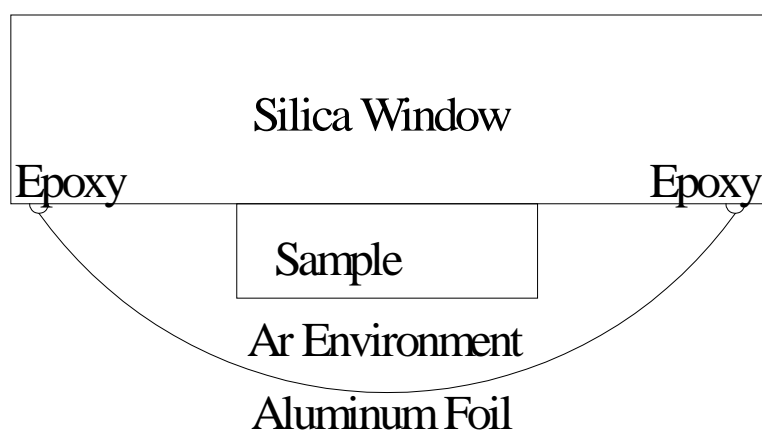
**Table 2 Half-cell states during each EIS measurement**

EIS Measurement	Half-Cell State
First	Virgin
Second	Discharged (0.5 V vs. Na/Na <sup>+</sup> )
Third	Charged (2.5 V vs. Na/Na <sup>+</sup> )
Fourth	Discharged (0.5 V vs. Na/Na <sup>+</sup> )
Fifth	Charged (2.5 V vs. Na/Na <sup>+</sup> )

## 2.4 Physical Characterization Methods

Physical characterization was performed to confirm the presence of an SEI. All samples for physical characterization were cycled vs. Na/Na<sup>+</sup> prior to measurements; after cycling, they were rinsed in DMC for 30 seconds twice and then vacuum dried in the Ar-filled glove box. The electrode samples utilized in the FT-IR and XPS measurements were at charged state (Na extraction), and the samples for the RAMAN

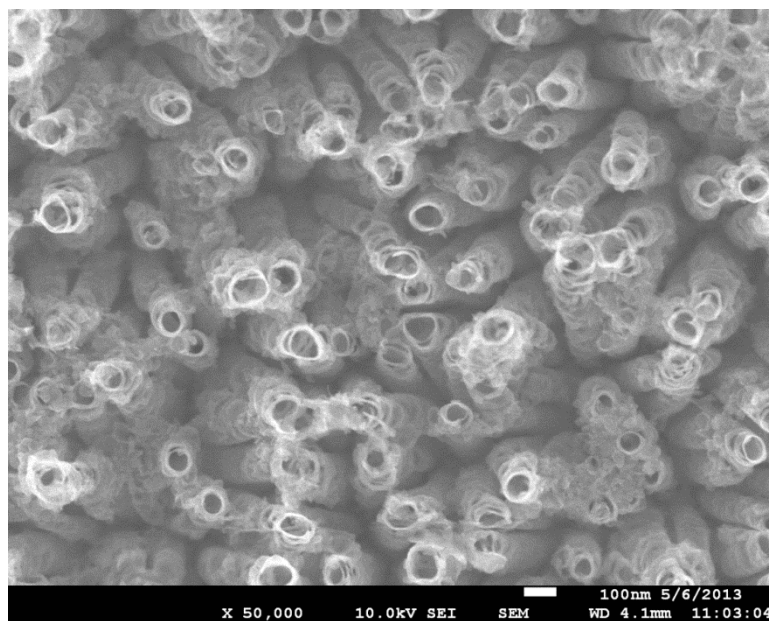
measurements were in a discharged state (Na insertion). After rinsing the electrodes, preparations were made for transport to testing facilities. For samples tested in open atmosphere, they were sealed for transport in Al foil pouches in the glove box. The RAMAN samples were hermetically sealed with epoxy in a pouch with an amorphous silica window to permit measurements while maintaining an inert Ar environment as seen in *Figure 2*.



**Figure 2** Sample prepared for RAMAN measurements in hermetically sealed pouch.

FT-IR measurements were made using a PerkinElmer Spectrum 100 in Attenuated Total Reflectance mode. The spectra were collected between 4000 and 600  $\text{cm}^{-1}$  with a resolution limit of 4  $\text{cm}^{-1}$ . FT-IR spectra were acquired at room temperature in open atmosphere. XPS was used to determine the binding states of the constituent elements at the electrode surface. The XPS measurements were carried out in a PHI VersaProbe II Scanning XPS Microprobe. Raman spectra were collected using a Horiba Jobin Yvon T64000 triple monochromator that utilized a liquid-nitrogen-cooled multi-channel coupled-charge-device detector. The probe beam used was a 325 nm ultraviolet laser. All Raman spectra were acquired at room temperature through the amorphous silica pouch window.

## CHAPTER THREE: RESULTS AND DISCUSSION

3.1 TiO<sub>2</sub> NT Characterization

**Figure 3** Top view of TiO<sub>2</sub> NTs in SEM

**Figure 3** shows an SEM image-top view of the NTs after anodization. The anodization process completely covers the foil surface with a visibly high density of NTs. The opening on the NTs is between 80 and 100 nm. The side view of the NTs is shown in **Figure 4**. The NTs are approximately 2.8  $\mu\text{m}$  tall. The ratio of opening to height is 1 to 28, which leads to very high surface area on the electrode. The wall thickness of the NTs is 5-10 nm, meaning that the diffusion distances for any Na-ions in the structure will be short.

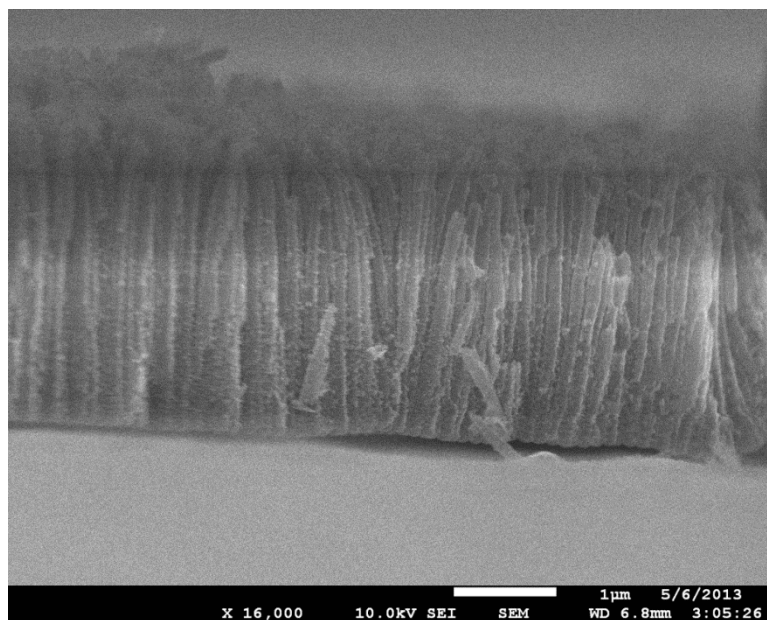


**Figure 4** Side view of TiO<sub>2</sub> NTs in SEM

### 3.2 Water Content in Electrolytes

The Karl Fischer titration results are seen in Table 3. The solvents used contain ppm levels of water. EC:PC has the least water, followed by EC:DMC, PC, EC:EMC, and EC:DEC. Water in the electrolytes has several potential problems. In a Na half-cell, the water in the electrolyte could react with the Na counter electrode. Water in the electrolyte could also cause reactions to occur in electrolyte solution that alter its behavior. The water also has the potential to alter the surface of the TiO<sub>2</sub> electrode. Altering that surface could have a dramatic effect on SEI formation, structure, and stability. Ideally the water content of the electrolyte will be below detection limits.

**Table 3** Results of Karl Fischer Titrations

Sample	Water Content (ppm)
PC	47
EC:PC	20
EC:DMC	21
EC:DEC	400
EC:EMC	>100

### 3.3 Electrochemical Characterization

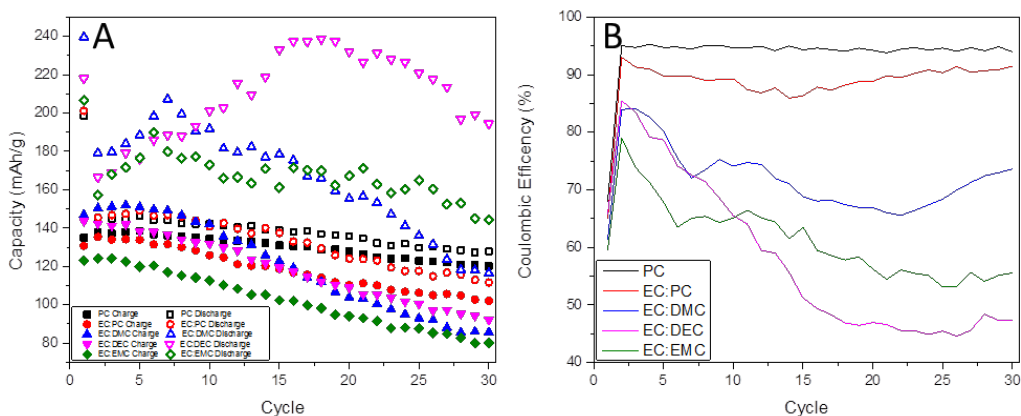


**Figure 5** Half-cells of TiO<sub>2</sub> NTs vs Na/Na<sup>+</sup>. A) Electrochemical capacity of the half cells. B) Coulombic efficiency of the half cells.

The half-cells were all cycled at a low current rate of 16 mA/g. The low current rate was used to allow the system to approach equilibrium conditions. **Figure 5A** shows the capacity of the TiO<sub>2</sub> NTs half-cells measured with the different electrolytes used. The TiO<sub>2</sub> NTs electrodes gradually lost capacity when cycled with each electrolyte. The electrode cycled with EC:EMC had the lowest charge capacity and Coulombic efficiency during testing. The poor performance of EC:EMC corresponds to high water content in the electrolyte. Using PC lead to the highest charge capacity retention among tested electrolytes. The difference between the charge and discharge capacities (indicated by Coulombic efficiency in **Figure 5B** suggests that there are side reactions occurring during cycling. This difference is most pronounced for the electrodes cycled with EC:DMC, EC:DEC, and EC:EMC.

**Figure 5B** shows that the Coulombic efficiency of most of the cells is generally low with exceptions of PC and EC:PC. The half-cell with PC has the highest Coulombic

efficiency, 94%. Electrodes cycled with EC:PC remained more than 85% efficient, while the rest had very poor efficiency and the corresponding loss of capacity.

*Figure 6* shows the voltage profiles for the electrodes on the first, second, and thirtieth cycles. The observed monotonically linear sloping voltage curves during discharge and charge in all samples indicate a solid solution mechanism. There are some similar features seen in the behavior of each of the cells. In the first cycle of each cell, the discharge profile appears wavy. The ridges are an indication that there are side reactions taking place in each of the cells. In *Figure 6*, the PC and EC:PC data show that the ridges do not appear in either the second or thirtieth cycles, evidence that the side reactions are forming a stable SEI.

In *Figure 6*, the data for the EC:DMC, EC:DEC, and EC:EMC show that the ridges are still present after the first cycle. Though fainter, the presence of ridges indicates that the side reactions occurring during cycling are not forming a stable SEI. An unstable SEI would be dissolving during charging and consuming more energy every time the half-cell is discharged. There is an accompanying loss of capacity with the SEI seen in the half-cells using EC:DMC, EC:DEC, and EC:EMC, which is evidence that the SEI formed is parasitic.

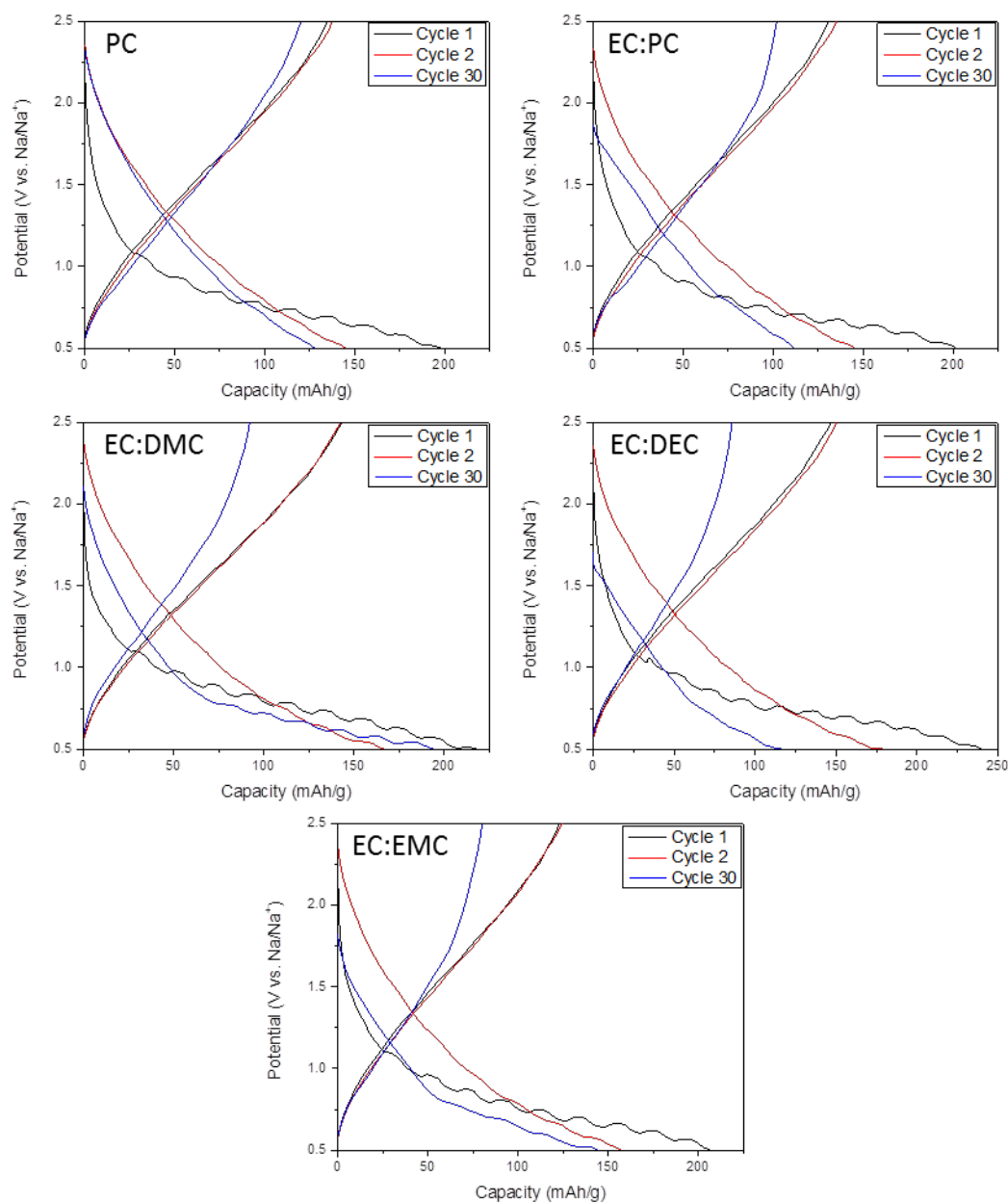
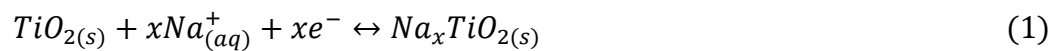


**Figure 6** Voltage profiles of the measured electrochemical performance on cycling the half-cells. Displayed are the 1<sup>st</sup>, 2<sup>nd</sup>, and 30<sup>th</sup> cycles. All electrolytes tested are reported here.

*Figure 7* shows the CV data corresponding to the cells. The expected reaction is written as follows:



This reaction describes the insertion/extraction of Na-ions into and out of the amorphous TiO<sub>2</sub>. CV is used to obtain reaction information. When plotting the current against the voltage, several features may become visible including the redox reactions that occur and any changes in the reactions that occur between cycles. In *Figure 7*, there is a clearly visible cathodic peak at approximately 0.75 V vs Na/Na<sup>+</sup> and a clearly visible corresponding anodic peak near 0.8 V vs Na/Na<sup>+</sup> on the cathodic curve for all samples. Zhao *et al.* have shown that in this potential range the Na ions begin to diffuse into or out of the TiO<sub>2</sub> NTs<sup>70</sup>. Xiong *et al.* have shown that at higher potentials the mechanism for charge transfer at the interface is capacitive-limited, while as the potential is reduced the charge transfer mechanism changes to a mixture of diffusion and surface capacitance<sup>14</sup>. The current data shows the peaks where diffusion is expected to be seen, along with an indication that there is activity at higher potentials.

Furthermore, the noticeable difference between the anodic and cathodic curves of the first cycle and the subsequent cycles indicates that there are side reactions occurring at the interface. The presence of moisture in the electrolyte may indicate that the H<sub>2</sub>O was decomposing. González *et al.* have shown that the downward facing tail at low potential indicates H<sub>2</sub> gas evolution in an aqueous solution<sup>45</sup>. This would suggest that the other product of H<sub>2</sub>O decomposition is the OH<sup>-</sup> ion. The expected reaction is as follows



The presence of hydroxide ions at the interface will be important later in the discussion. This is not the only potential side reaction occurring during cycling.

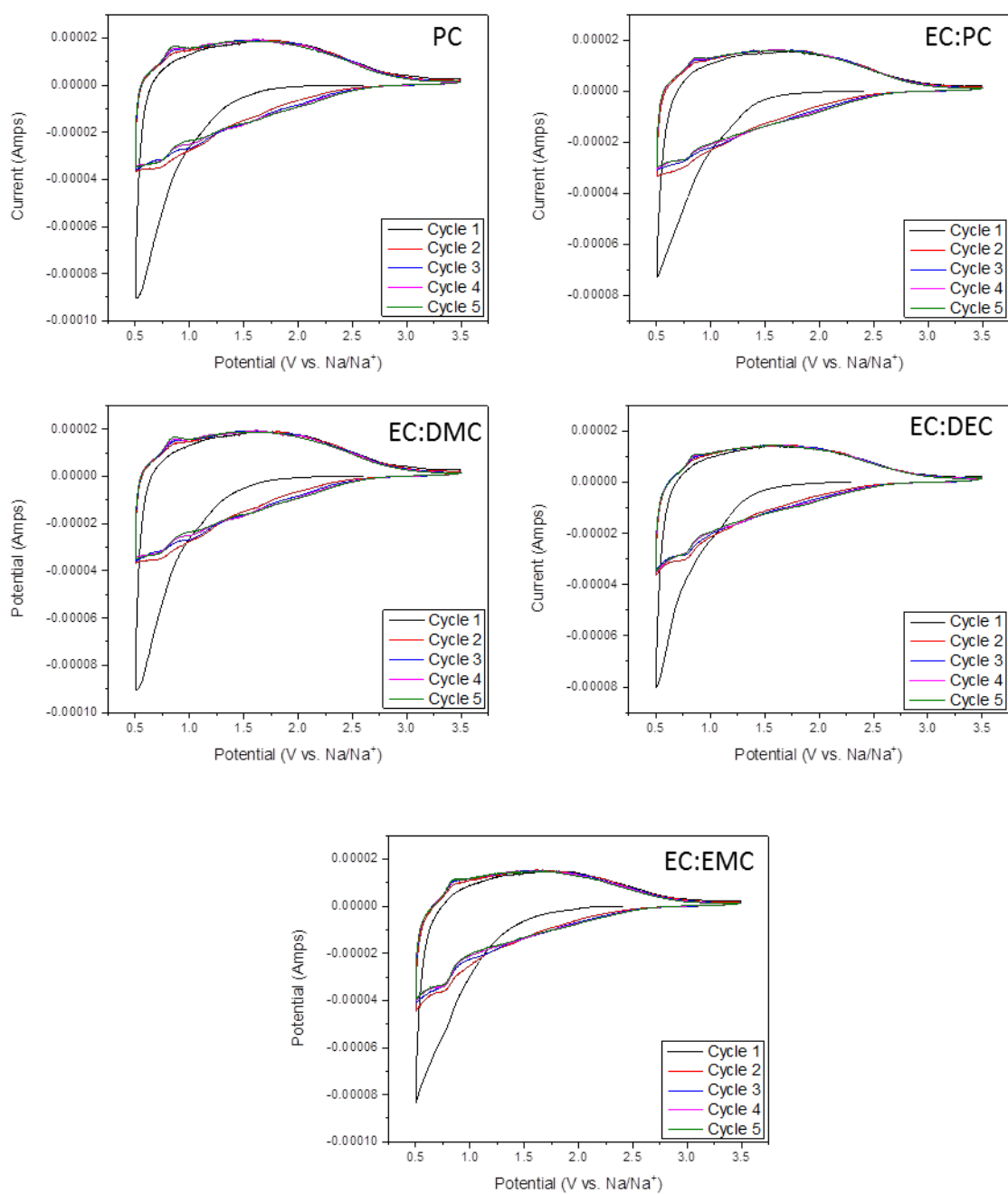


**Figure 7** Cyclic Voltammetry Data, all electrolytes tested are reported here.

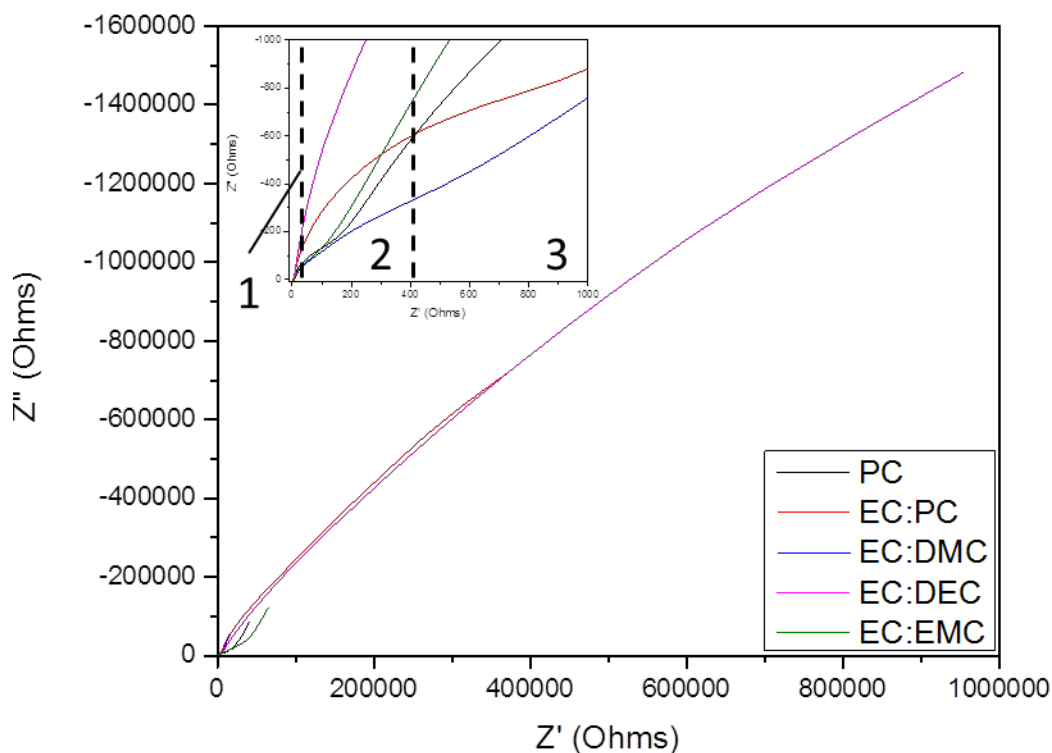


**Figure 8** EIS measurements of the uncycled half-cells. Insert shows the origin in greater detail. Section 1 is the high frequency region. The high frequency region describes the behavior of the bulk electrolyte. Section 2 is the medium frequency region. The medium frequency region shows the interface and interface reactions. Section 3 is the low frequency region, which indicates the diffusion in the solid electrode.

*Figure 8* presents the Nyquist plots from the EIS measurements of the uncycled half-cells with each electrolyte. EIS was used to study electrode processes, electrode/electrolyte interfaces, and ion mobility in the electrolyte by measuring the electrical impedance. In a typical Nyquist plot of a specific electrode-electrolyte system, the intercept of a semicircle at high frequency usually represents the resistance of the system (contact resistance, electrolyte resistance, etc.); semicircle(s) at medium frequency arise from SEI formation and charge transfer processes across the interface; and a  $45^\circ$  line at low frequency is due to the ion diffusion in the solid. The area of the

TiO<sub>2</sub> NT electrode was kept the same in all systems tested, hence the impedance in each system can be directly compared. Any changes in the bulk electrolyte will alter ionic diffusion and be seen at the intercept. The insert in **Figure 8** shows that as-prepared electrodes with various electrolytes all have similar system resistance as indicated by the intercepts along  $Z'$ . The smaller diameter of a depressed semicircle in EC:PC compared with other electrolyte systems indicates facile charge transfer at the electrode/electrolyte interface. Clearly there are differences at the interface for the different electrolytes even before cycling the half-cells.

**Figure 9** reports the EIS results from a TiO<sub>2</sub> NT electrode in PC at different states of charge. As seen in the **Figure 9**, intercepts at high frequencies, there is no discernable change in the bulk electrolyte during cycling. The apparent change occurs during the first discharge of the half-cell. The semicircle is an indication of a SEI formation. After the first discharge, the interface appears to continue to change as seen by the differences in the diameter of the semicircle in the EIS data in the successive cycles, but the changes seen are much less drastic. We noticed that the impedance of the SEI layer increases slightly in the second discharge compared to the initial discharge, which might be due to the instability of the formed SEI layer but the effect is not significant. The impedance of the SEI layer at the charged state (both first and second charges) is larger than those at the discharged states, which might be related to the concentration of Na ions inside the SEI layer. Diffusion behavior varies as the half-cell is discharged and then charged. The EIS data for the half-cell with PC are consistent with the results from the capacity and CV data that has been previously reported. An unstable SEI is forming on the TiO<sub>2</sub> NT electrode during cycling. That the instability of the SEI is minor further agrees with the

capacity measurements reported in *Figure 5* because the half-cell with PC electrolyte has high Coulombic efficiency and a corresponding high retention of capacity.

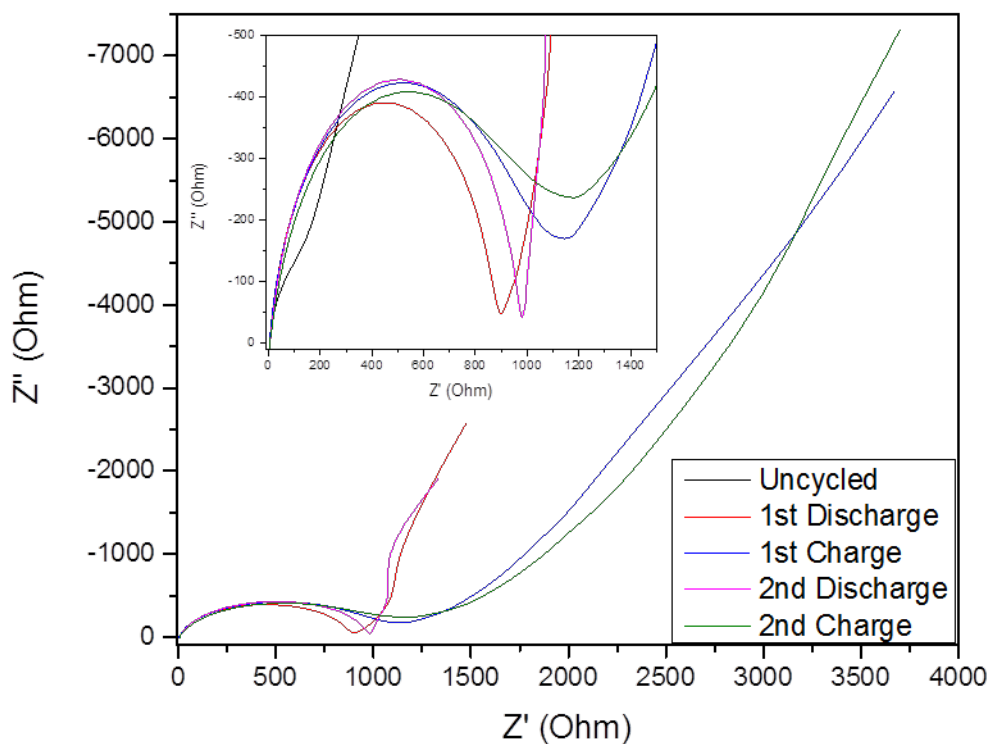


**Figure 9** EIS measurements for half-cell with PC electrolyte. The insert shows the origin with greater detail.

*Figure 10* reports the EIS results from a  $\text{TiO}_2$  NT electrode in EC:PC at different states of charge. The similar position of the intercepts of the impedance spectra for the electrode at different states of charge indicates that the bulk electrolyte properties do not vary when the electrode was cycled. The diameter of the semicircles at different states of charge does not vary significantly, which indicates that the SEI layer formed in EC:PC is more stable than the PC system. However, the impedance of the SEI layer in the EC:PC system is higher than that in the PC system, which explains the lower charge capacity of EC:PC in comparison with PC.

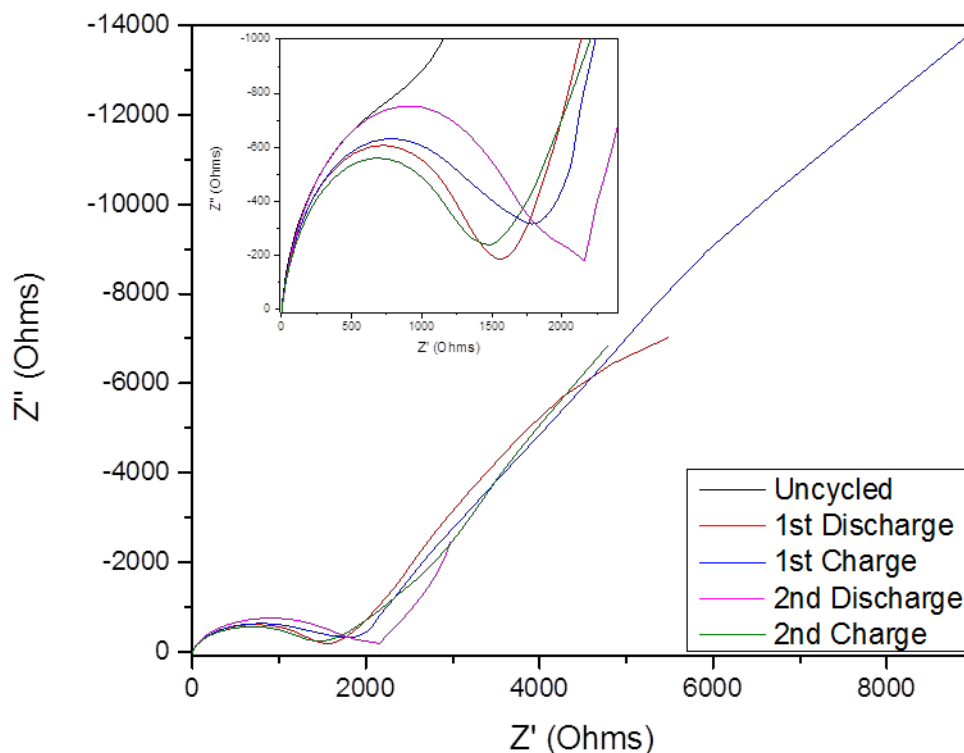


**Figure 10** EIS measurements for half-cell with EC:PC electrolyte. The insert shows the origin with greater detail.

The impedance results of the EC:EMC system are presented in **Figure 11** and they follow a similar pattern that is seen in the PC and EC:PC systems. An SEI layer might have formed at the electrode surface during cycling and the impedance of the possible SEI layer is smaller compared to the PC and EC:PC system. The impedance at the charged states is larger than that at the discharged states, indicating that the concentration of Na ions in the SEI layer might play an important role in the charge transfer across the electrode/electrolyte interface. In addition, the much larger impedance of the SEI layer at the charged states could explain the low Coulombic efficiency in the EC:EMC shown in **Figure 5B**.

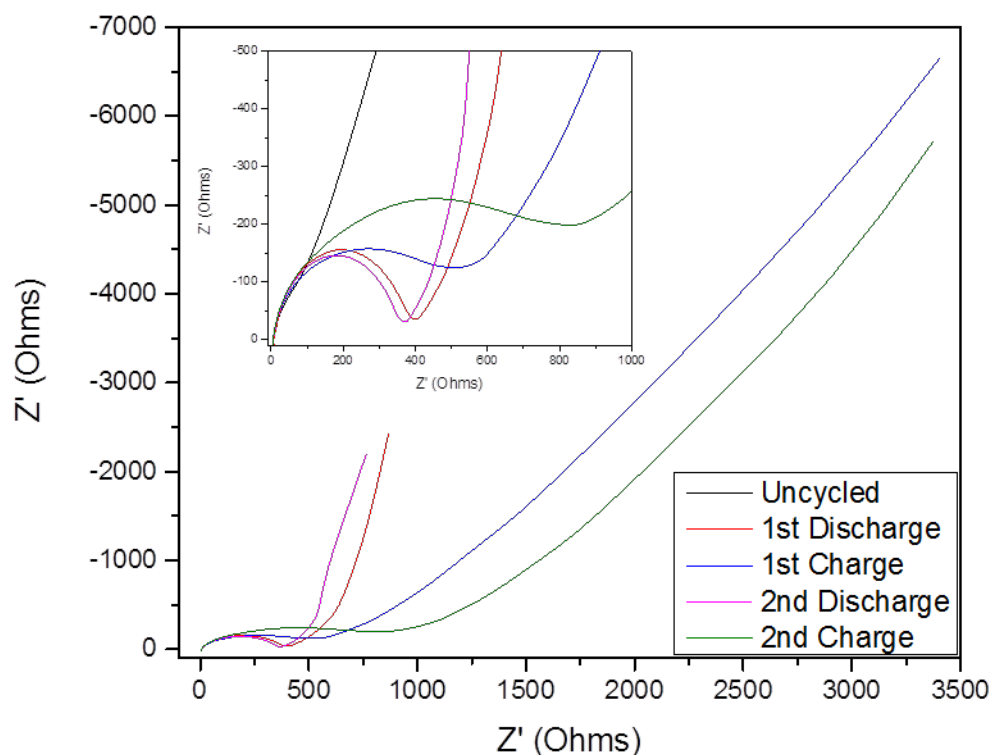


**Figure 11** EIS measurements for half-cell with EC:EMC electrolyte. The insert shows the origin with greater detail.

**Figure 12** presents the EIS results from a  $\text{TiO}_2$  NT electrode with EC:DMC at different states of charge. **Figure 12** shows that although there is no change in the resistance of bulk EC:DMC electrolyte indicated by the intercepts of each plot, there is a change in the behavior of the SEI. In contrast to the previous three systems (PC, EC:PC, and EC:EMC), the impedance of the SEI layer decreases in the second discharge compared to the initial discharge, which indicates cycling the Na ion in and out helps to facilitate the ionic transport inside the SEI layer. On the other hand, it is likely that the SEI layer is not stable and may dissolve and reform on each cycle. The EIS data is consistent with the results from the capacity and CV data (**Figure 5** and **Figure 7**) that the SEI is highly unstable and parasitic.

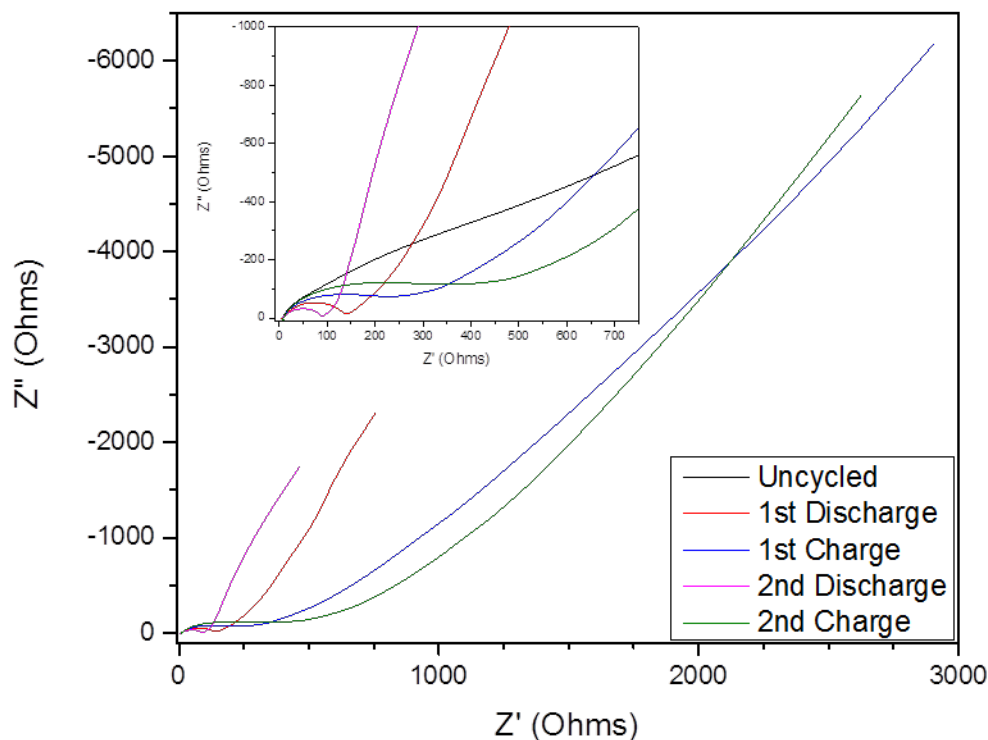


**Figure 12** EIS measurements for half-cell with EC:DMC electrolyte. The insert shows the origin with greater detail.

The Nyquist plots of the  $\text{TiO}_2$  NT electrode in the EC:DEC system, shown in **Figure 13**, follows the pattern of behavior seen in the half-cell with EC:DMC. A close look at the semicircles in the **Figure 13** insert shows that this interface has the least stable SEI of the electrolytes tested. Major changes are seen every time the half-cell is charged or discharged. This corroborates and in part explains the data reported in **Figures 5** and **6** in which the half-cell with EC:DEC electrolyte has the lowest Coulombic efficiency and has a significant loss of capacity during cycling. An SEI that is continually forming and dissolving would impede the operation of the half-cell.

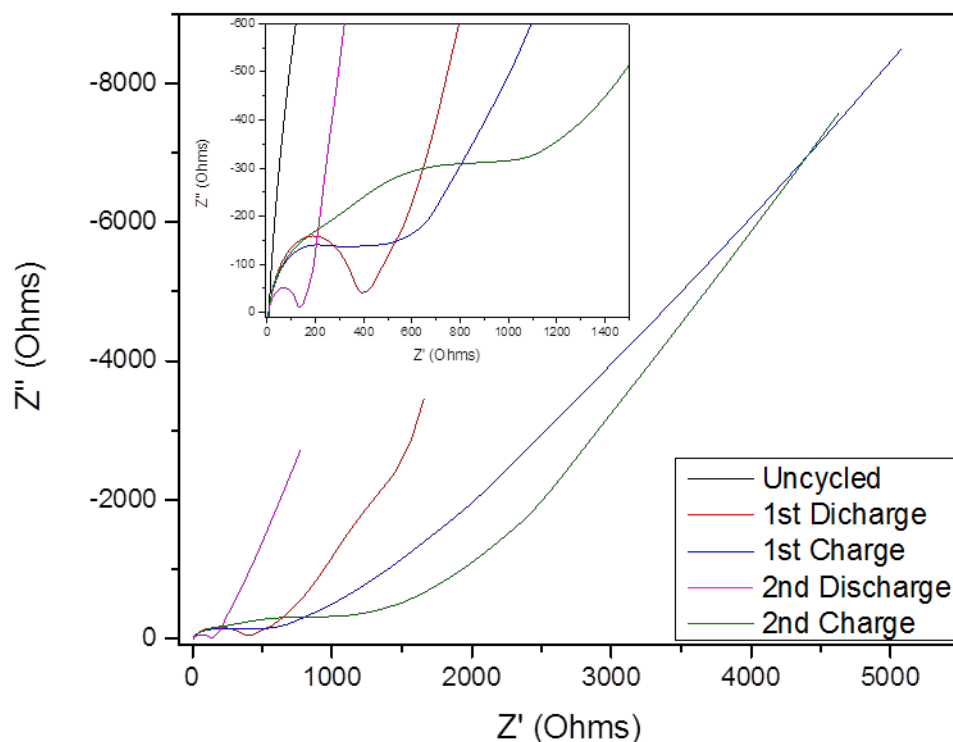


**Figure 13** EIS measurements for half-cell with EC:DEC electrolyte. The insert shows the origin with greater detail.

In summary, side reactions are occurring at the electrode/electrolyte interface. The Coulombic efficiencies reported indicate the extent of the side reactions. In the PC and EC:PC systems, the side reactions appear to stabilize after the initial cycle, while in the EC:DMC, EC:DEC, and EC:EMC systems, the side reactions do not stabilize. The voltage profiles are consistent with the results from the Coulombic efficiencies, showing side reactions for every system during the first cycle, but no evidence of side reactions in the second and thirtieth cycles for the PC and EC:PC systems. CV also shows a noticeable difference between the initial cycle and subsequent cycles. The EIS tests provide further evidence for the presence of the side reactions by the change in diameter of the semicircles (magnitude of the SEI impedance) after the first discharge of the half-

cells. These side reactions are most likely cause for the formation of SEIs on the electrode surface.

### 3.4 Physical Characterization

In the previous section, we demonstrated that side reactions are occurring at the electrode surface. We concluded that SEIs are forming on electrodes as a result of the side reactions that have been observed. It is possible that the side reactions in each system are producing some other reaction products, however, this is unlikely. Because the only variable in the experiment is the electrolyte solvent, the likely cause of the side reactions could be a reaction of the salt at the electrode surface. Our physical characterization methods focused on identifying the reactant products at the surface to determine the behavior of the salt.

We have discussed the possibility that some of the water in the electrolyte is decomposing into H<sub>2</sub> gas and OH<sup>-</sup> ions. Another possible reaction of the water at the TiO<sub>2</sub> NT surface is hydration. Li *et al.* have demonstrated that the TiO<sub>2</sub> hydration leads to a surface structure of Ti(OH)<sup>+</sup> on which other H<sub>2</sub>O and OH<sup>-</sup> molecules can then attach themselves by hydrogen bonding<sup>71</sup>. Salt stability will have a significant impact on the side reactions and any SEI formation. ClO<sub>4</sub><sup>-</sup> is normally a stable ion despite being a powerful oxidant, however research indicates that when in the presence of titanous ions and ethanolic solutions it is rapidly reduced to Cl<sup>-</sup><sup>72</sup>. A similar reduction reaction could be occurring on the TiO<sub>2</sub> in carbonate liquids given the water content of the electrolytes if the water in the electrolyte is hydrating the TiO<sub>2</sub> NT surface and thereby creating similar conditions for the reaction.

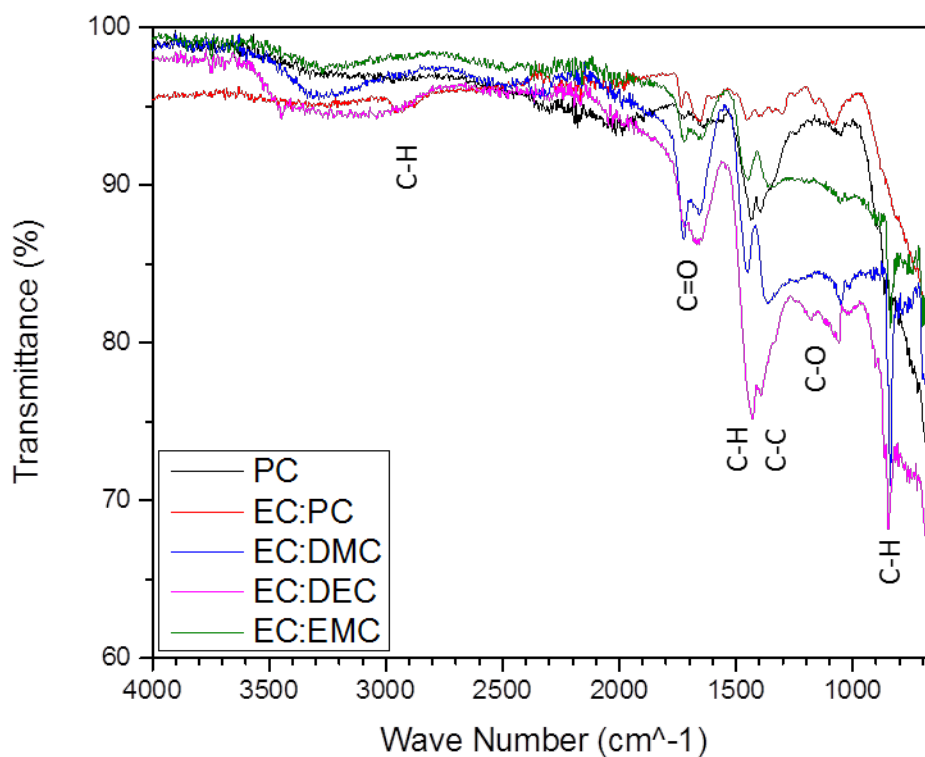


**Figure 14** FT-IR spectra for the electrodes after one complete discharge/charge cycle for each of the electrolytes tested.

**Table 4** Bonding information of the FT-IR peaks seen in the measured spectra

Peaks ( $\text{cm}^{-1}$ )	Bond
2800-3000	C-H <sup>73,74</sup>
1700-1800	C=O <sup>73-77</sup>
1400-1500	C-H <sup>74,78</sup>
1400-1500	C-C <sup>79</sup>
1000-1270	C-O <sup>74,75,78</sup>
840-850	C-H <sup>73,78</sup>
840	C-Cl <sup>80,81</sup>

**Figure 14** displays the data gathered in FT-IR measurements and **Table 4** provides the peak identities. The peaks between 1000 and 2000  $\text{cm}^{-1}$  and 2800-3000  $\text{cm}^{-1}$  correspond to organic molecules, C-O and C-H bonds. The appearance of such peaks

could possibly be from residual electrolyte on the surface of the electrode. C-C bonds are seen between 1400 and 1500  $\text{cm}^{-1}$ . C=O bonds are seen at 1700 to 1800  $\text{cm}^{-1}$ . Each of these bonds is present in the electrolyte, however the electrodes were rinsed and then vacuum dried to drive off the electrolyte. The C-H, C-O, C=O, and C-C bonds seen confirm the electrochemical evidence of an SEI that has been already discussed in the previous section. There are also peaks for each of the electrolytes, except for EC:PC, at  $\sim 840 \text{ cm}^{-1}$ , which are clearly seen in *Figure 15*. *Figure 15* shows the low wavenumber data in greater detail where the C-Cl bond can be seen clearly.

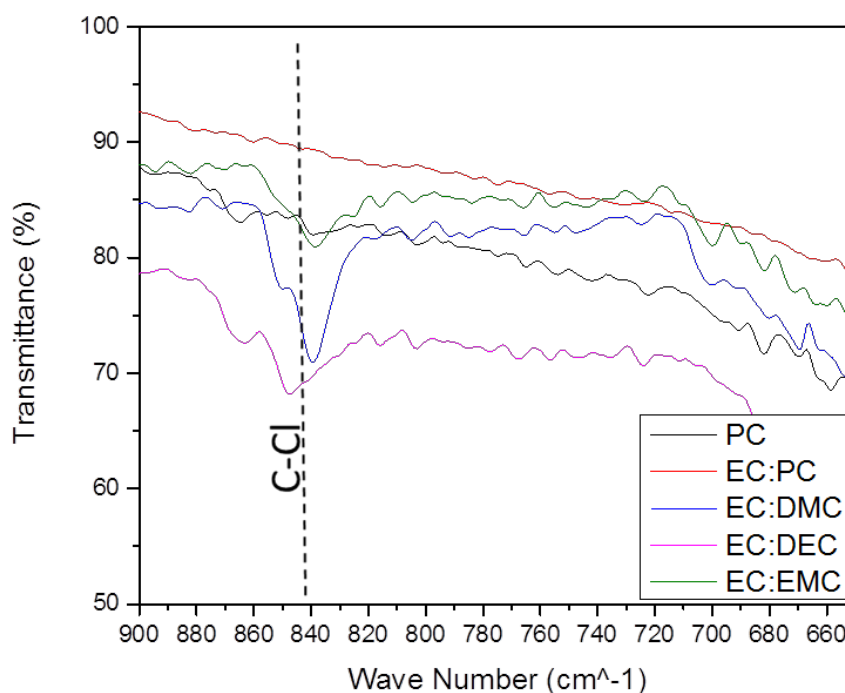
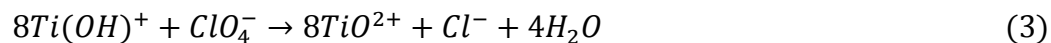


**Figure 15** FT-IR data at low wavenumbers. The dotted line marks the C-Cl bond.

The  $840 \text{ cm}^{-1}$  peak corresponds to a C-Cl bond. The  $\text{ClO}_4^-$  ion is the only source of Cl in the assembled half-cells. The presence of C-O bonds alone would not indicate that the  $\text{ClO}_4^-$  ions were decomposing as O is present in the carbonate solvents as well.

The C-Cl bond, however, acts as clear evidence that the  $\text{ClO}_4^-$  ions may decompose. The C-Cl bond is also further evidence that an SEI is forming. The decomposition is expected to take place at the surface of the  $\text{TiO}_2$  NT electrode. Earley and Tofan have shown that titanous ions act as a catalyst for decomposition of  $\text{ClO}_4^-$  ions<sup>72</sup>. The reaction that Earley and Tofan reported is:



If the water in the electrolyte is hydrating the surface of the  $\text{TiO}_2$  NTs, then the surface conditions will be similar to the ethanolic solution reported by Earley and Tofan and would allow the reaction to proceed as indicated in equation 3. Because the water present in the electrolyte is only present at ppm levels, it is possible that the whole surface of the electrode is not hydrated prior to cycling. The water produced through the possible side reaction indicated by equation 3 during cycling may then further hydrate the electrode surface and cause more perchlorate decomposition. Equation 3 as written indicates that water present with the  $\text{Cl}^-$  ions at the  $\text{TiO}_2$  surface will result in  $\text{ClO}_4^-$  ions. The decomposition reaction will compete with the formation of  $\text{ClO}_4^-$  ions and will be controlled by the diffusion of water and the SEI formation. The forming SEI could prevent surface hydration and stop perchlorate decomposition, which would account for the observed capacity of the  $\text{TiO}_2$  NT electrodes in the PC and EC:PC systems. The forming SEI also may not prevent surface hydration, which would explain the behavior seen in the EC:DMC, EC:DEC, and EC:EMC systems.

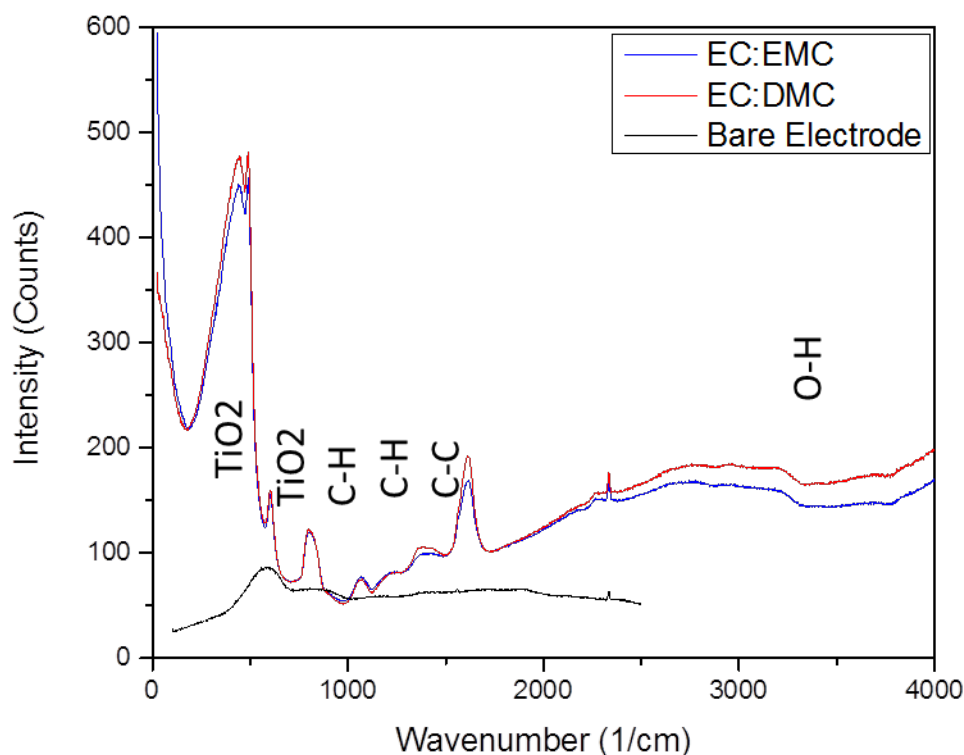


**Figure 16** Raman spectra for TiO<sub>2</sub> electrodes in charged state. Two electrolytes were tested, EC:EMC and EC:DMC.

**Figure 16** shows the Raman spectra collected from TiO<sub>2</sub> NT electrodes cycled in EC:DMC and EC:EMC electrolytes as well as the Raman spectra of virgin TiO<sub>2</sub> nanotubes. The peaks at 440, 490, and 560 cm<sup>-1</sup> are seen in all of the samples, including the bare electrode, uncycled TiO<sub>2</sub> NTs. The peak at 2330 cm<sup>-1</sup> is also seen in all samples, including the bare TiO<sub>2</sub>. The peaks 440, 490, and 560 cm<sup>-1</sup> are characteristic of the TiO<sub>2</sub> substrate<sup>82-87</sup>. The peaks from 560-1150 cm<sup>-1</sup> have a component from the TiO<sub>2</sub> substrate<sup>85</sup> but are more pronounced because there are some overlapping C-H vibrations<sup>88</sup>. The SEI is seen in the peaks 1225 and 1370 cm<sup>-1</sup>, which indicate C-H bonding<sup>88</sup>. The 1370 cm<sup>-1</sup> peak is broad and may be an amalgamation of a C-H peak with a C-C peak<sup>89</sup>. Farther out, the peaks from 3200-3600 cm<sup>-1</sup> indicate the presence of O-H

bonding<sup>90</sup>. As the  $\text{ClO}_4^-$  ions decompose, the free O may be reacting with the organics at the electrode-electrolyte interface and replacing H in some of the C bonds. This would leave free H that would readily react with free O.

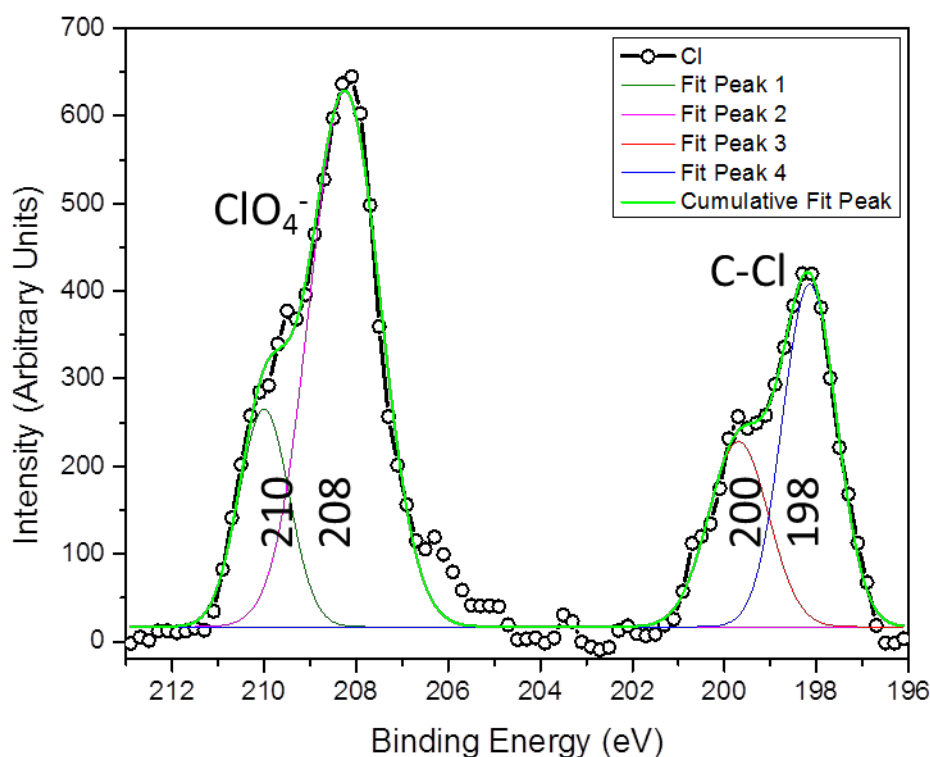


**Figure 17** XPS data from half-cell with PC electrolyte, focused on the Cl spectra collected. The black line and circles shows the data collected by the XPS. The fitted peaks 1-4 are the identified peaks in the spectra and the cumulative peak fit in green shows that the fit matches the data.

The XPS results in **Figure 17** confirm that the  $\text{ClO}_4^-$  ion is decomposing. The higher energy peaks at 208 and 210 eV on the left are the  $\text{ClO}_4^-$  ion<sup>91</sup> while the lower energy peaks correspond to a C-Cl bond<sup>92-94</sup>. The perchlorate ion is the sole source of Cl in the system. If the  $\text{ClO}_4^-$  ion was stable and showed no signs of decomposition, we would expect to see only one set of peaks to correspond with the binding energy of the perchlorate ion. However, the presence of a second set of peaks in the XPS spectra both

shows that the  $\text{ClO}_4^-$  ion is unstable and indicates that there is a second compound with Cl present after cycling. The FT-IR spectra agree with this analysis, indicating the presence of a C-Cl bond. Because Cl is forming bonds with C after the perchlorate ions have decomposed, the side reactions observed in the electrochemical testing are probably forming a SEI. The performance of the  $\text{TiO}_2$  NT electrodes is dependent on the stability and the mobility of Na ions in the SEI.

## CHAPTER FOUR: CONCLUSIONS

In summary, we have found that all five of the electrolytes tested PC, EC:PC, EC:DMC, EC:DEC, and EC:EMC show indications of formation of an SEI layer when the TiO<sub>2</sub> NT electrodes were cycled. The SEI that forms on the TiO<sub>2</sub> NT electrodes in connection with EC:DMC, EC:DEC, and EC:EMC are clearly parasitic and detrimental to the operation of the half-cell. The SEI formed on the TiO<sub>2</sub> NT electrodes with PC and EC:PC are more stable and show more promise for actual use in a Na-ion battery. The superior performance is a combination of the high dielectric constants of the solvents and the low water content of the electrolytes, which leads to a more stable SEI. EC:PC is the most stable solvent mixture for an electrolyte used with a TiO<sub>2</sub> NT electrode. The superior capacity retention of EC:PC is due in part to the minimal moisture present, as well as the highest solution dielectric constant.

Also, although NaClO<sub>4</sub> is a stable salt for use in batteries it is unsuitable for application with TiO<sub>2</sub> electrodes. In our study, the ClO<sub>4</sub><sup>-</sup> ion decomposed readily and contributed to the buildup of a parasitic SEI. At the present time, it is unclear if the ClO<sub>4</sub><sup>-</sup> ion decomposition is caused by the moisture present in the solvents or only exacerbated by it, however, in either case, the use of a ClO<sub>4</sub><sup>-</sup> ion in this system is not recommended.

Future work on this project should include researching a salt more suitable for the TiO<sub>2</sub> NT electrodes. The new electrolyte salt should be stable, having no components that will readily decompose. The salt should also not contain any components that will promote side reactions at the interface. NaPF<sub>6</sub> would be an excellent starting material for

the new salt research, because it is inexpensive, readily available, and there have already been several studies that show it has potential. The solvents should also be investigated in an anhydrous state. Studying the solvent performance after dehydration should lead to improvements in the performance of all of the solvents. Dehydration could be achieved by mixing the solvent and then adding pure Na metal to react with and remove any water present. Dehydrating the solvents and testing them with  $\text{NaClO}_4$  will indicate whether or not the moisture in the solvents was the cause of the  $\text{ClO}_4^-$  ion decomposition. Finally, solvent additives should be investigated. In other systems, like electrodes of carbon or metal oxides, electrolyte additives such as fluoroethylene carbonate have increased the stability of the SEI formed and improved capacity retention on cycling.

## REFERENCES

1. A. Yoshino, K. Sanechika, and T. Nakajima, 1987.
2. U. G. Survey, *Mineral Commodities Surveys*, 2012.
3. V. Palomares, P. Serras, I. Villaluenga, K. B. Hueso, J. Carretero-González, and T. Rojo, *Energy Environ. Sci.*, 2012, **5**, 5884.
4. P. Thomas, J. Ghanbaja, D. Billaud, H. Poincare, and I. Nancy, *Electrochim. Acta*, 1999, **45**, 423–430.
5. D. a. Stevens and J. R. Dahn, *J. Electrochem. Soc.*, 2000, **147**, 1271.
6. R. Alcántara, J. M. Jiménez Mateos, and J. L. Tirado, *J. Electrochem. Soc.*, 2002, **149**, A201.
7. P. Thomas, D. Billaud, I. Nancy, and B. P. Vandoeu, *Electrochim. Acta*, 2002, **47**, 3303–3307.
8. R. Alcántara, P. Lavela, G. F. Ortiz, and J. L. Tirado, *Electrochem. Solid-State Lett.*, 2005, **8**, A222.
9. S. Komaba, W. Murata, T. Ishikawa, N. Yabuuchi, T. Ozeki, T. Nakayama, A. Ogata, K. Gotoh, and K. Fujiwara, *Adv. Funct. Mater.*, 2011, **21**, 3859–3867.
10. S. Wenzel, T. Hara, J. Janek, and P. Adelhelm, *Energy Environ. Sci.*, 2011, **4**, 3342.
11. a. Ponrouch, a. R. Goñi, and M. R. Palacín, *Electrochem. commun.*, 2013, **27**, 85–88.
12. L. Ji, M. Gu, Y. Shao, X. Li, M. H. Engelhard, B. W. Arey, W. Wang, Z. Nie, J. Xiao, C. Wang, J.-G. Zhang, and J. Liu, *Adv. Mater.*, 2014, **26**, 2901–8.
13. L. D. Ellis, T. D. Hatchard, and M. N. Obrovac, *J. Electrochem. Soc.*, 2012, **159**, A1801–A1805.
14. H. Xiong, M. D. Slater, M. Balasubramanian, C. S. Johnson, and T. Rajh, *J. Phys. Chem. Lett.*, 2011, **2**, 2560–2565.

15. L. W. Shacklette, T. R. Jew, and L. Townsend, *J. Electrochem. Soc.*, 1985, **135**, 2669–2674.
16. Y. Cao, L. Xiao, W. Wang, D. Choi, Z. Nie, J. Yu, L. V Saraf, Z. Yang, and J. Liu, *Adv. Mater.*, 2011, **23**, 3155–60.
17. D. J. Kim, R. Ponraj, A. G. Kannan, H.-W. Lee, R. Fathi, R. Ruffo, C. M. Mari, and D. K. Kim, *J. Power Sources*, 2013, **244**, 758–763.
18. H. Liu, H. Zhou, L. Chen, Z. Tang, and W. Yang, *J. Power Sources*, 2011, **196**, 814–819.
19. H. Fei, X. Liu, H. Li, and M. Wei, *J. Colloid Interface Sci.*, 2014, **418**, 273–6.
20. N. Recham, J.-N. Chotard, L. Dupont, K. Djellab, M. Armand, and J.-M. Tarascon, *J. Electrochem. Soc.*, 2009, **156**, A993.
21. P. Moreau, D. Guyomard, J. Gaubicher, and F. Boucher, *Chem. Mater.*, 2010, **22**, 4126–4128.
22. H. Zhuo, X. Wang, A. Tang, Z. Liu, S. Gamboa, and P. J. Sebastian, *J. Power Sources*, 2006, **160**, 698–703.
23. N. Yabuuchi, M. Kajiyama, J. Iwatate, H. Nishikawa, S. Hitomi, R. Okuyama, R. Usui, Y. Yamada, and S. Komaba, *Nat. Mater.*, 2012, **11**, 512–7.
24. S. Oh, S. Myung, C. S. Yoon, J. Lu, J. Hassoun, B. Scrosati, K. Amine, and Y. Sun, *Nano Lett.*, 2014, **14**, 0–6.
25. M. Sathiya, K. Hemalatha, K. Ramesha, J.-M. Tarascon, and A. S. Prakash, *Chem. Mater.*, 2012, **24**, 1846–1853.
26. X. Xia and J. R. Dahn, *Electrochem. Solid-State Lett.*, 2012, **15**, A1.
27. I. D. Gocheva, M. Nishijima, T. Doi, S. Okada, J. Yamaki, and T. Nishida, *J. Power Sources*, 2009, **187**, 247–252.
28. R. Alc, J. M. Jim, and P. Lavela, *Electrochem. commun.*, 2001, **3**, 637–640.
29. X. Zhou, X. Zhu, X. Liu, Y. Xu, Y. Liu, Z. Dai, and J. Bao, 2014.
30. Y. Wen, K. He, Y. Zhu, F. Han, Y. Xu, I. Matsuda, Y. Ishii, J. Cumings, and C. Wang, *Nat. Commun.*, 2014, **5**, 4033.
31. P. R. Abel, M. G. Fields, A. Heller, and C. B. Mullins, 2014.

32. K. Shiva, H. B. Rajendra, and A. J. Bhattacharyya, *Chempluschem*, 2015, **80**, 516–521.
33. Y. Yang, X. Yang, Y. Zhang, H. Hou, M. Jing, Y. Zhu, L. Fang, Q. Chen, and X. Ji, *J. Power Sources*, 2015, **282**, 358–367.
34. H. Hou, M. Jing, Y. Yang, Y. Zhu, L. Fang, W. Song, C. Pan, X. Yang, and X. Ji, 2014, **c**.
35. X. Xie, D. Su, K. Kretschmer, J. Zhang, B. Sun, and G. Wang, *Nano Energy*, 2015, **13**, 208–217.
36. J. Billaud, J. Cle, A. R. Armstrong, P. Rozier, C. P. Grey, and P. G. Bruce, 2014, 2–7.
37. J. R. Kim and G. G. Amatucci, *Chem. Mater.*, 2015, 150318130732008.
38. S. Guo, P. Liu, H. Yu, Y. Zhu, M. Chen, M. Ishida, and H. Zhou, *Angew. Chem. Int. Ed. Engl.*, 2015, 1–7.
39. Z. L. Brown, S. Smith, and M. N. Obrovac, *J. Electrochem. Soc.*, 2014, **162**, A15–A20.
40. Y. Dong, H. Wei, W. Liu, Q. Liu, W. Zhang, and Y. Yang, *J. Power Sources*, 2015, **285**, 538–542.
41. H.-Y. Li, C.-H. Yang, C.-M. Tseng, S.-W. Lee, C.-C. Yang, T.-Y. Wu, and J.-K. Chang, *J. Power Sources*, 2015, **285**, 418–424.
42. I. Hasa, D. Buchholz, S. Passerini, and J. Hassoun, *ACS Appl. Mater. Interfaces*, 2015.
43. W. Wang, S. Wang, H. Jiao, P. Zhan, and S. Jiao, *Phys. Chem. Chem. Phys.*, 2015, **17**, 4551–4557.
44. M. Moradi, Z. Li, J. Qi, W. Xing, K. Xiang, Y.-M. Chiang, and A. M. Belcher, *Nano Lett.*, 2015, 150406094951004.
45. J. R. Gonzalez, R. Alcantara, F. Nacimiento, G. F. Ortiz, and J. L. Tirado, *J. Electrochem. Soc.*, 2014, **162**, A3007–A3012.
46. L. Wu, D. Bresser, D. Buchholz, and S. Passerini, *J. Electrochem. Soc.*, 2014, **162**, A3052–A3058.
47. D. Wu, X. Li, B. Xu, N. Twu, L. Liu, and G. Ceder, *Energy Environ. Sci.*, 2015, **8**, 195–202.

48. P. J. P. Naeyaert, M. Avdeev, N. Sharma, H. Ben Yahia, and C. D. Ling, 2014.
49. Y. Ge, H. Jiang, J. Zhu, Y. Lu, C. Chen, Y. Hu, Y. Qiu, and X. Zhang, *Electrochim. Acta*, 2015, **157**, 142–148.
50. J. Hou, J. Song, Y. Niu, C. Cheng, H. He, Y. Li, and M. Xu, *J. Solid State Electrochem.*, 2015, 0–4.
51. J. Lee, Y. Chen, Y. Zhu, and B. D. Vogt, 2014.
52. B. Kang and G. Ceder, *Nature*, 2009, **458**, 190–3.
53. K. Zaghib, J. B. Goodenough, a. Mauger, and C. Julien, *J. Power Sources*, 2009, **194**, 1021–1023.
54. G. Ceder and B. Kang, *J. Power Sources*, 2009, **194**, 1024–1028.
55. J. Chong, S. Xun, X. Song, P. Ridgway, G. Liu, and V. S. Battaglia, *J. Power Sources*, 2012, **200**, 67–76.
56. A. Ponrouch, E. Marchante, M. Courty, J.-M. Tarascon, and M. R. Palacín, *Energy Environ. Sci.*, 2012, **5**, 8572.
57. A. Ponrouch, R. Dedryvère, D. Monti, A. E. Demet, J. M. Ateba Mba, L. Croguennec, C. Masquelier, P. Johansson, and M. R. Palacín, *Energy Environ. Sci.*, 2013, **6**, 2361.
58. A. Bhide, J. Hofmann, A. K. Dürr, J. Janek, and P. Adelhelm, *Phys. Chem. Chem. Phys.*, 2014, **16**, 1987–98.
59. C. Vidal-Abarca, J. L. Tirado, A. V. Chadwick, M. Alfredsson, and E. Kelder, *J. Power Sources*, 2012, **197**, 314–318.
60. S. Komaba, T. Ishikawa, N. Yabuuchi, W. Murata, A. Ito, and Y. Ohsawa, *ACS Appl. Mater. Interfaces*, 2011, **3**, 4165–4168.
61. G. Kamath, R. W. Cutler, S. a. Deshmukh, M. Shakourian-Fard, R. Parrish, J. Huether, D. P. Butt, H. Xiong, and S. K. R. S. Sankaranarayanan, *J. Phys. Chem. C*, 2014, **118**, 13406–13416.
62. L. Wu, D. Buchholz, D. Bresser, L. Gomes Chagas, and S. Passerini, *J. Power Sources*, 2014, **251**, 379–385.
63. P. V. Kamat, *J. Phys. Chem. C*, 2012, **116**, 11849–11851.

64. H. Xiong, H. Yildirim, E. V Shevchenko, V. B. Prakapenka, B. Koo, M. D. Slater, M. Balasubramanian, S. K. R. S. Sankaranarayanan, P. Greeley, S. Tepavcevic, N. M. Dimitrijevic, P. Podsiadlo, C. S. Johnson, and T. Rajh, *J. Phys. Chem. C*, 2012, **116**, 3181–3187.
65. J. M. Macak, B. G. Gong, M. Hueppe, and P. Schmuki, *Adv. Mater.*, 2007, **19**, 3027–3031.
66. S. Berger, R. Hahn, P. Roy, and P. Schmuki, *Phys. Status Solidi*, 2010, **247**, 2424–2435.
67. J. L. Schaefer, Y. Lu, S. S. Moganty, P. Agarwal, N. Jayaprakash, and L. a. Archer, *Appl. Nanosci.*, 2011, **2**, 91–109.
68. K. Xu, 2004.
69. H. Xiong, H. Yildirim, P. Podsiadlo, J. Zhang, V. Prakapenka, J. Greeley, E. Shevchenko, K. Zhuravlev, S. Tkachev, S. Sankaranarayanan, and T. Rajh, *Phys. Rev. Lett.*, 2013, **110**, 078304.
70. L. Zhao, L. Qi, and H. Wang, *J. Power Sources*, 2013, **242**, 597–603.
71. G. Li, L. Li, J. Boerio-goates, and B. F. Woodfield, *J. Am. Chem. Soc.*, 2005, **127**, 8659–8666.
72. G. A. A. Joseph E. Earley Sr., Daniel C. Tofan, *ACS Symp.*, 1999, **39**, 90–92.
73. G. V. Zhuang, H. Yang, B. Blizanac, and P. N. Ross, *Electrochem. Solid-State Lett.*, 2005, **8**, A441.
74. S. Ramesh, K. H. Leen, K. Kumutha, and a K. Arof, *Spectrochim. Acta. A. Mol. Biomol. Spectrosc.*, 2007, **66**, 1237–42.
75. T. Matsushita, K. Dokko, and K. Kanamura, *J. Power Sources*, 2005, **146**, 360–364.
76. A. M. Stephan, T. P. Kumar, N. G. Renganathan, S. Pitchumani, and R. Thirunakaran, 2000, 80–87.
77. D. Lin-Vien, N. B. Colthup, W. G. Fateley, and J. G. Grasselli, *The Handbook of Infrared and Raman Characteristics Frequencies of Organic Molecules*, Academic Press Inc, San Diego, California, 1st Editio., 1991.
78. S.-W. Song and S.-W. Baek, *Electrochim. Acta*, 2009, **54**, 1312–1318.
79. K. Rajalakshmi and S. A. John, *Electrochim. Acta*, 2015, **165**, 268–276.

80. a. De Lorenzi, S. Giorgianni, and R. Bini, *Mol. Phys.*, 1999, **96**, 101–108.
81. M. Cai, L. Zhang, and L. Feng, *Chem. Eng. J.*, 2014, **244**, 188–194.
82. a. Orendorz, a. Brodyanski, J. Lösch, L. H. Bai, Z. H. Chen, Y. K. Le, C. Ziegler, and H. Gnaser, *Surf. Sci.*, 2006, **600**, 4347–4351.
83. a. Orendorz, a. Brodyanski, J. Lösch, L. H. Bai, Z. H. Chen, Y. K. Le, C. Ziegler, and H. Gnaser, *Surf. Sci.*, 2007, **601**, 4390–4394.
84. M. Zhang, M. Zhang, S. Shi, X. Song, and Z. Sun, *J. Alloys Compd.*, 2014, **591**, 213–217.
85. K. M. Deen, A. Farooq, M. A. Raza, R. Ahmad, and W. Haider, *J. Ind. Eng. Chem.*, 2015, **22**, 153–158.
86. M. Kubo, Y. Mantani, and M. Shimada, 2015, **48**, 292–299.
87. P. Shao, J. Tian, Z. Zhao, W. Shi, S. Gao, and F. Cui, *Appl. Surf. Sci.*, 2015, **324**, 35–43.
88. I. a. Belogorokhov, D. a. Mamichev, M. a. Dronov, V. E. Pushkarev, L. G. Tomilova, and D. R. Khokhlov, *Semiconductors*, 2010, **44**, 1044–1049.
89. a I. Alajtal, H. G. M. Edwards, and I. J. Scowen, *Anal. Bioanal. Chem.*, 2010, **397**, 215–21.
90. G. E. Walrafen, *J. Chem. Phys.*, 1970, **52**, 4176.
91. M. a. Amin, *Electrochim. Acta*, 2009, **54**, 1857–1863.
92. I. P. B, R. P. B, U. Narkiewicz, D. M. N, J. Anna, and B. B. Witkowski, 2013, **2013**.
93. A. L. Alpatova, M. J. Baumann, S. H. Davies, and S. J. Masten, 2013, 309–313.
94. T. J. Whitcher, K. H. Yeoh, C. L. Chua, K. L. Woon, N. Chanlek, H. Nakajima, T. Saisopa, and P. Songsiriritthigul, *Curr. Appl. Phys.*, 2014, **14**, 472–475.